Journal of Materials Chemistry B

Accepted Manuscript

ROYAL SOCIETY OF CHEMISTRY

www.rsc.org/materialsB

Journal of Material Chemistry B

ARTICLE

Synthesis of Silver Nanoparticles for the Dual Delivery of Doxorubicin and Alendronate to Cancer Cells

F. Benyettou,[a] R. Rezgui,[a] F. Ravaux,[b] T. Jaber,[a] K. Blumer,[a] M. Jouiad,[b] L. Motte,[c] J.-C. Olsen,[d] C. Platas-Iglesias,[e] M. Magzoub,[a] and A. Trabolsi[a]*

Received 00th January 20xx,
Accepted 00th January 20xx

DOI: 10.1039/x0xx00000x

www.rsc.org/

We present the synthesis of a silver nanoparticle (AgNP) based drug-delivery system that achieves the simultaneous intracellular delivery of doxorubicin (Dox) and alendronate (Ald) and improves the anticancer therapeutic indices of both drugs. Water, under microwave irradiation, was used as the sole reducing agent in the size-controlled, bisphosphonate-mediated synthesis of stabilized AgNPs. The AgNPs were coated with the bisphosphonate Ald, which templated nanoparticle formation and served as a site for drug attachment. The unreacted primary ammonium group of Ald remained free and was subsequently functionalized with either Rhodamine B (RhB), through amide formation, or Dox, through imine formation. The RhB-conjugated NPs (RhB-Ald@AgNPs) were studied in HeLa cell culture. Experiments involving the selective inhibition of cell membrane receptors were monitored by confocal fluorescence microscopy and established that macropinocytosis and clathrin-mediated endocytosis were the main mechanisms of cellular uptake. The imine linker of the Dox-modified nanoparticles (Dox-Ald@AgNPs) was exploited for acid-mediated intracellular release of Dox. We found that the Dox-Ald@AgNPs had significantly greater anti-cancer activity *in vitro* than either Ald or Dox alone. The Ald@AgNPs can accommodate the attachment of other drugs as well as targeting agents and therefore constitute a general platform for drug delivery.

1. Introduction

Cytotoxic drugs are used in cancer therapy to inhibit tumor growth and metastasis.[1] One of the most prescribed anticancer drugs is doxorubicin (Dox), which acts by intercalating DNA and inhibiting macromolecular biosynthesis. However, Dox has limited cellular uptake and a strong tendency to bind off-target macromolecules,[2] These drawbacks lead to low therapeutic indices and necessitate the use of large doses and repeated administration to achieve therapeutic efficacy. Unfortunately, such intensive treatment regimes cause severe side effects. One way to minimize the required dosage of Dox and to limit the severity of its side effects is to improve its cellular uptake. Another strategy is to administer Dox with drugs that act synergistically.[3] For example, Dox is significantly more effective against breast cancer when combined with alendronate (Ald), a potent bisphosphonate.[3,4] Furthermore, the use of Dox as part of a synergistic drug combination has the potential to delay the onset of Dox resistance.[4] Thus, a delivery vehicle that could facilitate simultaneous intracellular uptake of Dox and other drugs could lead to a highly effective cancer therapy.

Silver nanoparticles (AgNPs) have been used as effective drug delivery agents and have attracted special attention because of their intrinsic anticancer activity.[5] Various strategies have been developed for the preparation of biocompatible AgNPs, including micro-emulsion,[6] organic-water two-phase synthesis,[7] radiolysis,[8] and, the most common protocol, reduction in aqueous solution.[9] Despite its eco-friendly potential, the latter method uses an excess of reducing agent, such as citrate[10] or sodium borohydride,[11] which can be difficult to remove and/or cytotoxic.[12] Consequently, the development of AgNP syntheses that are both "green" and non-toxic remains an open challenge.

Here, we present a simple synthetic route to AgNPs that effectively deliver a synergistic combination of Dox and Ald to HeLa cells (Scheme 1). Our AgNPs have a coating of Ald molecules that are attached by chelating bisphosphonate moieties. This mode of Ald binding leaves the ammonium group of the drug free in solution and is supported by Fourier transform infrared (FTIR) spectroscopy as well as density functional theory (DFT) calculations. The ammonium group serves as an attachment site for either Rhodamine B (RhB), a hydrophilic, drug-like molecule, or Dox. RhB is attached by amide formation, and Dox, by imine formation. Both types of bond are pH sensitive and allow for intracellular release of RhB or Dox within the acidic microenvironment of late endosomes and lysosomes.

[a] *New York University Abu Dhabi, Abu Dhabi, United Arab Emirates.*
[b] *Masdar Institute of Science and Technology, Department of Mechanical and Materials Engineering, Abu Dhabi, United Arab Emirates.*
[c] *Université Paris 13, Sorbonne Paris Cité, Laboratoire CSPBAT, CNRS, (UMR 7244), F-93017, Bobigny, France.*
[d] *School of Sciences, Indiana University Kokomo, Kokomo, IN 46904, USA.*
[e] *Departamento de Química Fundamental, Universidade da Coruña, Campus da Zapateira, Rúa da Fraga 10, 15008 A Coruna, Spain.*
Electronic Supplementary Information (ESI) available: [details of any supplementary information available should be included here]. See DOI: 10.1039/x0xx00000x

To assess the efficacy of the system, we studied the *in vitro* cellular uptake of RhB-conjugated AgNPs (RhB-Ald@AgNPs) in HeLa cells and tracked the particles by monitoring RhB fluorescence. We then determined the toxicity of Dox-Ald@AgNPs in HeLa cells and quantified the synergistic effect of the Dox-Ald drug combination.

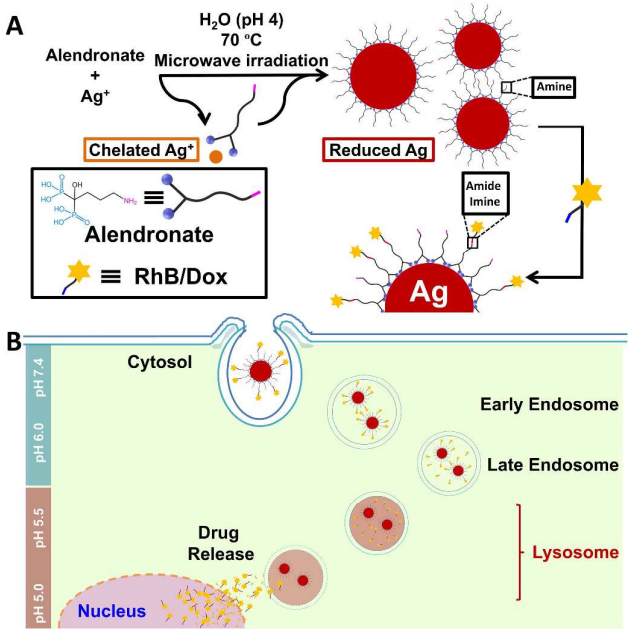

Scheme 1. (A) Schematic representation of Ald@AgNP formation and dye/drug conjugation. (B) Schematic representation of the uptake of drug-Ald@AgNPs into cells and drug cargo release.

2. Results and discussion

2.1. Synthesis and characterization of Ald@AgNPs

Previously reported syntheses of AgNPs typically require a stoichiometric amount of reducing agent, such as citrate[10] or sodium borohydride.[11] In this work, we used water as both solvent and reductant. The optimized synthetic procedure involves addition of an aqueous solution of silver nitrate (0.85 M, 1 mL) to an aqueous solution of Ald (0.15 M, 1 mL). The solution is heated by microwave (MW) irradiation for 15 minutes at pH 4 at a target temperature of 70 °C. A change in color of the solution from colorless to yellow indicates the formation of nanoparticles. The product is dialyzed for two days to remove unreacted starting materials.

UV–Vis spectroscopy, scanning electron microscopy (SEM), transmission electron microscopy (TEM), and dynamic light scattering (DLS) confirmed the formation of Ald@AgNPs and were employed to characterize the formation of metallic NPs in aqueous solution and to assess their stability.[13,14] UV–Vis spectroscopy is a reliable technique to authenticate the formation and stability of AgNPs in aqueous solution.[15] AgNPs usually exhibit a strong, broad absorption peak as a result of surface plasmon resonance. Our AgNPs showed an absorption maximum at 412 nm (Fig. 1A), which corresponds to a surface plasmon resonance typical of 11 nm NPs. The presence of this absorption maximum is also strong evidence for lack of NP aggregation. A SEM micrograph (Fig. 1B) shows spherical nanoparticles of 11 nm diameter. The particles are highly monodispersed and uniformly distributed as a result of fast and uniform microwave heating. High-resolution TEM (Fig. 1C and Supporting Information) confirmed the size of the particles and indicated that they are crystalline with the typical face-centered cubic structure of bulk silver.

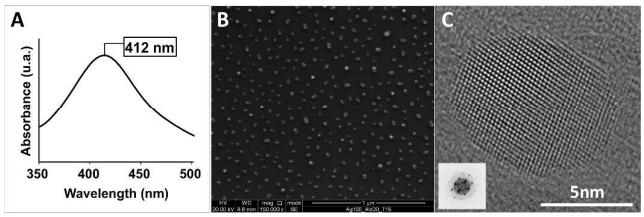

Fig. 1. Characterization of Ald@AgNP samples synthesized under MW irradiation and with [Ag] = 0.85 M, [Ald] = 0.15 M, t = 15 min, pH = 4 and at 70 C°. (A) Absorption spectrum, (B) SEM and (C) high-resolution TEM of Ald@AgNPs. (Inset of C: Fourier transform of particle along the (110) zone axis of face-centered cubic silver).

We measured the hydrodynamic size and the surface charge of the particles by using DLS. Both size and charge are good indicators of the aggregation state of NPs.[16] The hydrodynamic diameter at physiological pH (7.4) was found to be 20 nm, which is suitable for intracellular delivery applications.[17] The ζ-potential was found to be –37 mV as a consequence, in part, of the negatively charged state of Ald at this pH. The negative ζ-potential stabilizes the NPs by creating inter-particle electrostatic repulsions that prevent aggregation. This type of stability is a key feature. To avoid thrombosis upon intravenous injection the nanoparticles must not aggregate.

2.2. Surface characterization of Ald@AgNPs

FTIR and ^{31}P NMR spectroscopies, and DFT calculations were used to determine the mode of attachment of Ald to the surface of the NPs. Absorptions that correspond to the phosphonic acid group appear in the 850–1300 cm^{-1} fingerprint region and give an indicatation of the group's hydrogen-bonding and metal-binding interactions.[18] In the FTIR spectrum of free Ald (Fig. 2A), absorption bands consistent with phosphonic acid[19] are present at 1234, 1172, and 1127 cm^{-1} (ν, P=O), at 1047 and 1011 cm^{-1} (ν_s, ν_{as} of PO_3), and at 913 cm^{-1} (ν, POH), and the P=O and POH absorption bands are sharp. In contrast, in the spectrum of Ald@AgNPs (Fig. 2B) the P=O and POH absorptions merge to form one broad band centered at 1097 cm^{-1} and indicate that the phosphonate groups of Ald are strongly surface-associated. Such broadening and shifting is consistent with the results of previous studies that involved hydroxyapatite and silver and established that the P=O absorption band is quite sensitive to hydrogen bonding and metal coordination.[20]

The spectra also indicate that the ammonium group of Ald is largely unaffected by adsorption of the drug. The N–H bending bands appear at 1641 and 1540 cm^{-1} in the spectrum of free Ald and at 1636 and 1535 cm^{-1} in the spectrum of Ald@AgNPs. These data are consistent with a free ammonium group that projects away from the silver surface into solution.

Solution ^{31}P NMR experiments (Supporting Information) demonstrated that all Ald molecules on the surface of the nanoparticles are chemically equivalent: only one phosphorus resonance, which appears at 19.2 ppm, is present in the Ald@AgNPs spectrum. For free Ald, the resonance appears at 17.7 ppm.

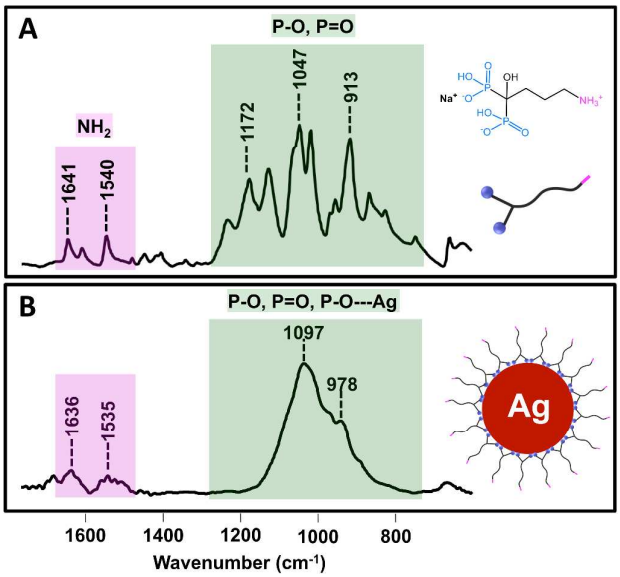

Fig. 2. Comparison of FTIR spectra of (A) free Ald and (B) Ald@AgNPs.

To gain greater insight about the interactions between AgNPs and Ald, we performed DFT calculations by using the hybrid meta generalized gradient approximation (hybrid meta-GGA) with the TPSSh exchange-correlation functional.[21] In these calculations (Fig. 3) we used the standard 6-311G(d,p) basis set for C, H, N, O, and P atoms, and Ag was described by using the ECP28MWB relativistic pseudopotential of Dolg *et al.*,[22] which includes 28 electrons in the core, together with the associated (8s7p6d2f1g)/[6s5p3d2f1g] basis set.[23] Bulk solvent effects (water) were included by using the integral equation formalism variant of the polarizable continuum model (IEFPCM). The selection of a reasonable model to gain information on the binding mode of small molecules to nanoparticles is not straightforward.[24] Several test calculations showed that the presence of two or three Ag atoms bound to Ald was an adequate approximation. The protonation state of Ald upon binding to the NPs is also not known, although the negative ζ-potential suggests the Ald moieties are negatively charged. Different test calculations performed with different protonation states of Ald indicated that the best agreement between experimental and calculated IR spectra were obtained when both the biphosphonate moiety and the amine group were monoprotonated, which leads to an overall –2 charge for the Ald unit. Full geometry optimization of the Ald@Ag_2^{2-} system provided a molecular structure in which each Ag atom is bound to three oxygen atoms of the Ald moiety with Ag–O distances of 2.32–2.56 Å, and a Ag–Ag distance of 2.92 Å. The latter value is in excellent agreement with those obtained experimentally by using EXAFS measurements (2.88 Å).[25] The simulated IR spectrum obtained with frequency calculations (half width at half height 25 cm^{-1}) is dominated by two absorption maxima at 1001 and 1181 cm^{-1} for P-O stretching vibrations that are similar to the experimental values of 978 and 1097 cm^{-1}. The band calculated at 688 cm^{-1} that arises from C-O-H and P-O-H bending vibrations (experimental value 669 cm^{-1}), and the bending vibrations of the -NH_3^+ group calculated at 1675 and 1533 cm^{-1} are also close to the experimental values (1636 and 1535 cm^{-1}). These *in silico* results must be considered carefully because of the complexity of the actual system and the simplicity of the model used. However, the overall good agreement between the observed and calculated IR spectrum in terms of shape and position of the main absorption bands suggests that Ald interacts with the AgNPs surface through the negatively charged bisphosphonate unit. Calculations performed on a model system that contained an amine group bound to Ag provide poor agreement with the experimental spectrum.

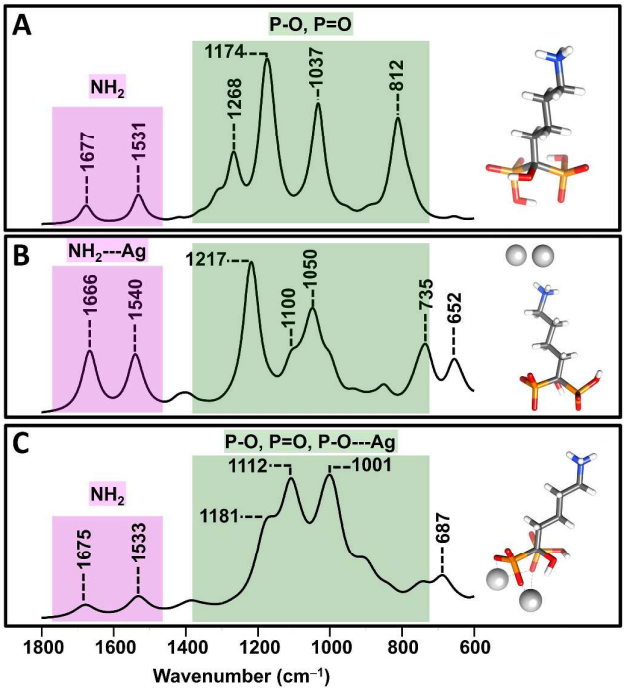

Fig. 3. Calculated FTIR spectra of (A) free Alendronate, (B) a model system of Ald@AgNPs with the ammonium group of Ald interacting with the AgNP surface and (C) a model system of Ald@AgNPs with the phosphonate groups of Ald interacting with the AgNP surface.

We quantified the number of Ald molecules on the AgNP surface using thermogravimetric analysis (TGA) which indicated a composition of 85.93% Ag and 9.07% Ald and which corresponds to an average of 4115 Ald molecules per NP and 84% surface coverage (see the Supporting Information for TGA and calculations). Such coverage density is in accordance with results previously reported for the adsorption of bisphosphonate onto the surface of iron-oxide NPs of similar diameter.[26]

2.3. Mechanism of Ald@AgNP formation

Ald@AgNPs are formed in our reaction mixtures despite the absence of stoichiometric amounts of conventional reducing

agents. In our method, we believe that microwave-irradiated water acts as the reducing agent. Vaks *et al.*[27] have proposed that water dissociates homolytically under the influence of 2.5–10 GHz MW radiation according to Equation 1. They suggest that, in contrast to conventional heating, MW irradiation produces shear and other mechanochemical forces in hydrogen-bonded networks of water molecules, and that these forces are necessary to produce the detected bond cleavage:

$$H_2O \leftrightarrows H^{\bullet}_{aq} + OH^{\bullet}_{aq} \qquad (1)$$

Among the several recombination reactions that they propose, the one described by Equation 2 is of particular interest:

$$H^{\bullet}_{aq} + OH^{-}_{aq} \leftrightarrows (H_2O)_{liq} + e^{-}_{aq} \qquad (2)$$

In this step, a highly reducing (–2.7 V) solvated electron is produced. Such an electron would be capable of reducing monovalent silver (E^0 Ag^+/Ag^0 = –1.8 V). Linnert *et al.*[28] have shown that, under similar conditions, it is possible to reduce silver ions with solvated electrons[29] generated by radiolysis. These authors suggest that silver atoms thus formed (Equation 3) react rapidly with Ag^+ ions to form Ag_2^+ species (Equation 4), which subsequently dimerize (Equation 5):

$$Ag^+ + e^{-}_{aq} \rightarrow Ag^0 \qquad (3)$$

$$Ag^0 + Ag^+ \rightarrow Ag_2^+ \qquad (4)$$

$$2\,Ag_2^+ \rightarrow Ag_4^{2+} \qquad (5)$$

We propose that steps similar to those described by Linnert *et al.*[28] and Ershov *et al.*[30] occur during the formation of Ald@AgNPs, in particular, that metallic Ag^+ ions are reduced by solvated electrons generated from water under MW irradiation.

In our control experiments, with conventional rather than microwave heating, the color change characteristic of NP formation was not observed after 15 minutes at 70 °C. Furthermore, no NPs were formed when Ald was absent from the reaction mixture. Both MW irradiation and Ald appear to be necessary for Ald@AgNP formation.

Linnert *et al.*[28] have reported that AgNP nucleation is greatly accelerated by polyphosphate (Pp), which increases the lifetime of Ag_2^+ by acting as a nucleating site for the formation of the metal (Equation 6). In the presence of Pp, stabilized small clusters form and give rise to an absorption band at 470 nm in the UV-visible spectrum. These small clusters grow into larger ones that have quasi-metallic properties and ultimately become AgNPs. Similarly, Ershov *et al.*[30] established that upon radiation-induced reduction of Ag^+ ions, the emergence of NPs is preceded by the appearance of stable, positively-charged clusters. In the absence of a stabilizing additive such as Pp, clusters exist in aqueous solution for only a short time (milliseconds to seconds) and do not lead to formation of NPs.

$$PpAg_4^{2+} + nH_2 + 2nAg^+ \rightarrow PpAg_{2n+4}^{2+} \qquad (6)$$

The UV-visible spectrum of Ald@AgNPs generated under our standard conditions in which Ald acts as a stabilizing additive is similar to those previously reported. Two absorption peaks (see the Supporting Information) confirm the stepwise mechanism of AgNP formation. The peak at 470 nm represents the small, positively charged silver clusters, and the peak at 411 nm represents the larger AgNPs.

To further investigate the involvement of the Ald phosphonate functionality in the NP templation process, we conducted three control experiments. In the first, we used a diesterified Ald,[31] in which the phosphonate groups are protected with phenyl groups and the ammonium group is free. In the second experiment, we performed the synthesis at pH 2, an acidity at which Ald has only one negatively charged phosphonate oxygen which is tied-up by its strong electrostatic interaction with the ammonium group.[32] In a third experiment, we adjusted the pH to 4 with triethylamine rather than NaOH. In this case, the negatively charged oxygen atoms of Ald are sterically hindered by ammonium cations and are not free to complex silver metal ions. In all three control experiments, no AgNP formation was observed. Together, these results argue against the direct involvement of an Ald's ammonium group in AgNP templation and bolster the case for the involvement of its bisphosphonate.

The experiments just described also rule-out the involvement of the Ald ammonium group in silver(I) reduction. In order to show that the bisphosphonate group of Ald is not involved in the reduction of the silver ions, we analyzed by ^{31}P NMR spectroscopy crude colloid solutions immediately after Ald@AgNP synthesis. If the bisphosphonate were to act as a reducing agent, it would degrade to form phosphates. However, no phosphates were detected in the reaction mixtures. Only one phosphorus resonance, at 19.2 ppm, was observed, and this signal corresponds to the two equivalent phosphorus atoms of the chelated bisphosphonate moiety. (See the Supporting Information for more details.)

The evidence suggests that Ald acts as a "microreactor" in which complexed silver ions are reduced. Silver(I) bisphosphonate complexes act as nucleation sites in which silver clusters and NPs grow. The bisphosphonate group of Ald controls the growth and size of the NPs and stabilizes the particles by chelation. This process is also consistent with the FTIR data (Fig. 2) which indicates the Ald molecules are adsorbed onto the surface of AgNPs through chelation by the bisphosphonate group.

2.4. Cell penetration studies

To study the mechanisms of cellular uptake and cargo release, we attached the fluorescent dye RhB to the Ald@AgNPs.

2.4.1. RhB conjugation

Under previously described conditions,[33] the carboxylic acid of the RhB was activated using carbodiimide chemistry and reacted with the ammonium group of surface-bound Ald (Fig. 4). The reaction mixture was purified by dialysis to remove any unreacted dye from the solution.

TGA was used to estimate the mass of RhB attached to the NPs and from this measurement it was determined that an average of 1054 RhB molecules were conjugated onto the surface of each particle (see the Supporting Information for calculations). With an average of 4115 Ald molecules per particle the conjugation efficiency of RhB was ~25%.

Unlabeled Ald@AgNPs are not intrinsically fluorescent at the RhB-specific excitation wavelength of λ_{ex} = 510 nm (see the Supporting

Information for details). At pH 7.4 and at λ_{ex} = 510 nm, the labeled sample of Ald@AgNPs (RhB-Ald@AgNPs) fluoresced less than an aqueous sample of free RhB of the same dye concentration (Fig. 4). This indicates that fluorescence quenching occurs within the RhB-Ald@AgNPs construct. Such quenching can be attributed to electronic interactions between the excited dye molecules and the NPs,[34] or to self-quenching of the dye on the surface of the particles where the effective concentration of the dye is relatively high.[35]

2.4.2. pH Triggered RhB release in solution

Acidic pH is a useful trigger for the selective release of anticancer drugs from NPs.[36] The pH of both primary and metastasized tumors is lower than that of normal tissue.[37] Furthermore, pH can change in cancer cells during endocytosis, dropping to 5.0–6.0 in late endosomes, or to 4.0–5.0 in lysosomes.[37]

We lowered the pH of a solution of RhB-Ald@AgNPs to 5.4. As shown in Fig. 4, the solution's fluorescence was dramatically enhanced after 24 hours relative to that of a sample that was kept at physiological pH (7.4). Such enhancement demonstrates that release of the dye from the silver nanocarriers is pH-sensitive. Release of the RhB chromophore could be the result of i) cleavage of the amide linkage that connects RhB and Ald or ii) dissociation of the bisphosphonate of Ald from the silver surface. ^{31}P NMR spectroscopic studies indicated (Figure S5) that acidification can cause Ald to dissociate from Ald@AgNPs. Either mechanism, amide cleavage or bisphosphonanate dissociation, would lead to diffusion of the RhB chromophore away from the surface of RhB-Ald@AgNPs and therefore to enhanced fluorescence. Both mechanisms are probably occurring.

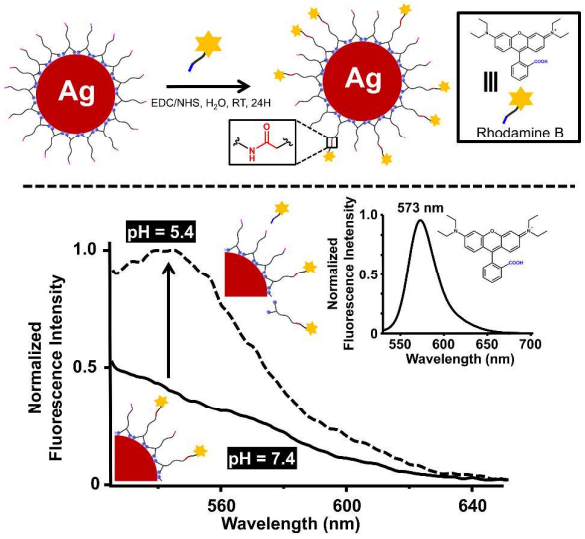

Fig. 4. Top: Schematic representation of the attachment of RhB to Ald@AgNPs using coupling agents 1-ethyl-3-(3-dimethylaminopropyl)carbodiimide (EDC) and N-hydroxysuccinimide (NHS). Bottom: Fluorescence emission spectra of RhB-Ald@AgNPs at pH 7.4 (solid curve) and after 24 hours of acidic hydrolysis at pH 5.4 (dashed curve). Inset: Fluorescence emission spectrum of RhB in water at room temperature with λ_{ex} = 510 nm.

2.4.3. Internalization pathway studies in HeLa cells

In vitro experiments with RhB-Ald@AgNPs were performed to determine the mechanism and kinetics of NP uptake into HeLa cells, which are a commonly used model for primary and metastatic human tumors.

2.4.3.1. Kinetics of cellular uptake

HeLa cells were incubated with RhB-Ald@AgNPs ([Ag] = 0.1 ?M, [RhB] = 2 μM), and cellular uptake of NPs was monitored by measuring the total amount of fluorescence accumulated within the cells over time using confocal microscopy.[38] Immediately following addition of the RhB-Ald@AgNPs to the cell medium (t = "0"), fluorescence of the dye was undetectable as a result of quenching at the NP surface. However, once the NPs were internalized, fluorescence increased over time and reached a plateau after 2 h (see the Supporting Information). Uptake half-time was estimated to be 77 ± 3 min for RhB-Ald@AgNPs. No fluorescence was observed within cells incubated with free RhB at the same concentration. These experiments demonstrate that Ald@AgNPs can function as a vehicle for intracellular delivery of small-molecule cargo.

2.4.3.2. Intracellular delivery and drug release mechanisms

The mechanisms by which macromolecules enter cells can be divided into two broad categories: i) passive mechanisms of internalization, such as direct translocation, which are energy independent,[39] and ii) active mechanisms, such as endocytosis, which are energy dependent.[40] We determined the relative amounts of RhB-Ald@AgNPs internalized by passive versus active mechanisms by measuring the fluorescence intensity emitted from cells that were incubated with NPs for 2 h at either 4 or 37 °C. At 4 °C, all active cellular processes, including endocytosis, are inhibited. At 4°C the fluorescence intensity emitted from incubated cells was 18% of that emitted from cells incubated at 37 °C (Fig. 5 and the Supporting Information). This difference indicates that, although a significant fraction of RhB-Ald@AgNPs is internalized by passive mechanisms, the predominant mechanisms are active ones.

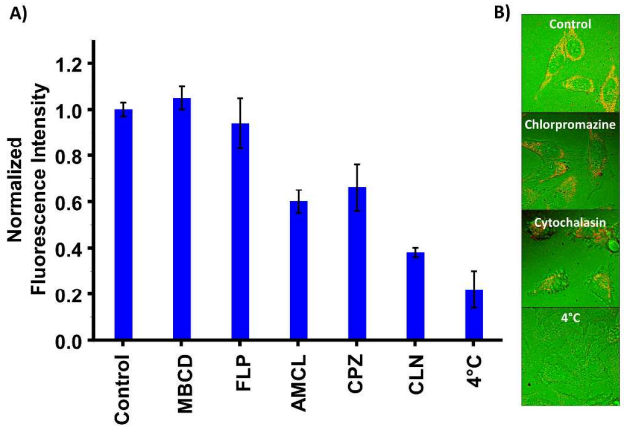

Fig. 5. Mechanism(s) of cellular internalization of RhB-Ald@AgNPs in HeLa cells. A) Effect of endocytotic inhibitors on cellular uptake of RhB-Ald@AgNPs. B) Confocal images after 2 h incubation ([Ag] = 0.1 μM, [RhB] = 2 μM). The experiment at 4 °C indicates an active

internalization pathway. Methyl-β-cyclodextrin (MBCD) and filipin (FLP) did not affect NP uptake. The inhibition of fluorescence by cytochalsin D (CLN), chlorpromazine (CPZ) and ammonium chloride (AMCl) indicates that macropinocytosis and chlathrin-mediated endocytosis are the major pathways of RhB-Ald@AgNP internalization. Red fluorescence in the confocal images indicates that the RhB cargo was efficiently released into lysosomes.

To determine the nature of the active entry mechanism(s) and their relative contribution to overall cellular uptake, chemical inhibitors for the various endocytic pathways were used (Fig. 5). The cells were treated with various inhibitors for 30 minutes prior to addition of NPs. The amount of fluorescence accumulated within the cells was monitored over 2 h following incubation with the fluorescent NPs and subsequently imaged with confocal microscopy. Fig. 5A shows the effect of the endocytic inhibitors on the amount of intracellular fluorescence relative to the control cells. Methyl-β-cyclodextrin and filipin, which are inhibitors of lipid raft synthesis and caveolin-dependent endocytosis, respectively, did not affect uptake of NPs because the total intracellular fluorescence value was close to that obtained for the control cells. However, addition of chlorpromazine, which is an inhibitor of clathrin-mediated endocytosis, resulted in a decrease in the overall fluorescence (30%) for RhB-Ald@AgNPs, which indicates that NP internalization occurs partly through clathrin-dependent endocytosis. Addition of cytochalsin D, an inhibitor of macropinocytosis, resulted in the greatest reduction in intracellular fluorescence (60%) relative to control cells. This observation indicates that macropinocytosis is the major pathway for internalization of NPs. Greulich *et al.*[41] also showed that macropinocytosis and clathrin-dependent endocytosis are the primary uptake mechanisms of AgNPs.

Finally, cells were treated with ammonium chloride, which inhibits lysosomal acidification. In the absence of acidification, intracellular fluorescence is 38% lower relative to the control. This decrease indicates that release of RhB molecules from the nanocarriers occurs as a result of breakage of the amide bond induced by the late endosomes/lysosomes' acidic (pH 5.0) microenvironment (Fig. 5). Thus, following cellular internalization of the RhB-Ald@AgNPs, mainly through macropinocytosis and clathrin-mediated endocytosis, the dye is released from the NPs in endo-lysosomal compartments as a result of their acidic microenvironment.

2.5. Dox conjugation, pH-triggered release and anti-proliferative activity against HeLa cells

Encouraged by the results of the RhB internalization studies, the ability of Ald@AgNPs to deliver Dox to HeLa cells was investigated and cell growth inhibition by the delivered drug was monitored.

Dox was attached to the surface of Ald@AgNPs by imine bond formation. Imine bond formation between free Ald and free Dox is supported by FTIR spectroscopy (Figure S1). TGA was used to estimate the mass of Dox attached to the NPs and an average of 682 Dox molecules were calculated to be attached to each particle (see Supporting Information for calculations). With an average of 4115 Ald molecules per particle, the conjugation efficiency of Dox was ~17%.

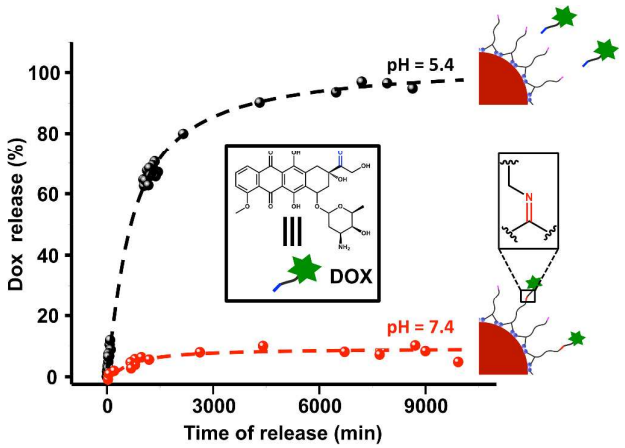

Fig. 6. *In vitro* Dox release profiles for Dox-Ald@AgNPs conducted over seven days at 37 °C and either pH 7.4 (red curve) or pH 5.4 (black curve). Schematic representations show the imine linkage that breaks under acidic conditions to release Dox.

Dox release from Dox-Ald@AgNPs was monitored over time by measuring Dox fluorescence in solution. Two aqueous samples were analyzed: one at physiological pH (7.4) and the other at a pH typically found within late endosomes and lysosomes (5.4). Fig. 6 shows the drug release profiles of the two samples. A small amount (~9%) of Dox was released over seven days at pH 7.4, whereas up to 95% of the drug was released at pH 5.4 over the same period.

The release of Dox from the NPs resulted from acid-promoted hydrolysis of the imine-linkage between Dox and Ald. We anticipate that the pH-sensitive Dox-Ald@AgNPs will exhibit limited premature drug-release in the bloodstream (pH 7.4), but will effectively kill cancer cells following cell internalization and Dox release within endocytic compartments at pH 6.5–4.5. Such a mechanism has the potential to increase drug efficacy and limit side effects.

Confocal laser scanning microscopy was used to determine the intracellular localization of Dox-Ald@AgNPs following uptake by endocytosis. HeLa cells were incubated with Dox-Ald@AgNPs for 3 h at 37 °C. After incubation, Dox was found to be distributed within the cytoplasm (Fig. 7), which indicates that Dox is released from endolysosomal compartments after endocytosis. The facile release of Dox into the cytoplasm is highly advantageous and makes Ald@AgNPs well-suited for intracellular drug delivery.

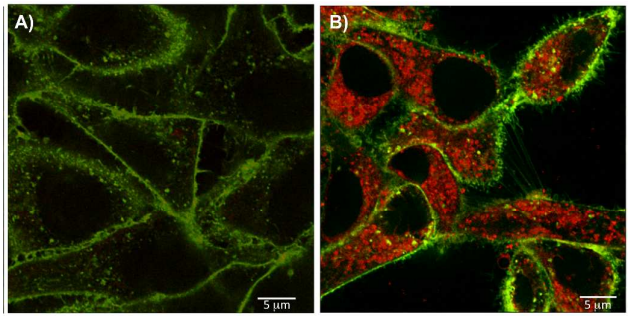

Fig. 7. Confocal images of HeLa cells incubated for 3 h at 37 °C with (A) phosphate buffered saline as a control or (B) Dox-Ald@AgNPs,

which are seen distributed evenly in the cytosol and appear red as a result of Dox fluorescence ([Ag] = 0.1 μM, [RhB] = 1.2 μM). Cell membranes are labeled with the green dye Alexa Fluor® 488.

The anti-tumor effect of Dox-Ald@AgNPs on HeLa cells was also evaluated. Inhibition of HeLa cell growth by free Ald, starch-coated AgNPs,[42] Ald@AgNPs or Dox-Ald@AgNPs was measured after 48 h incubation as a function of either Ald or Dox concentration.

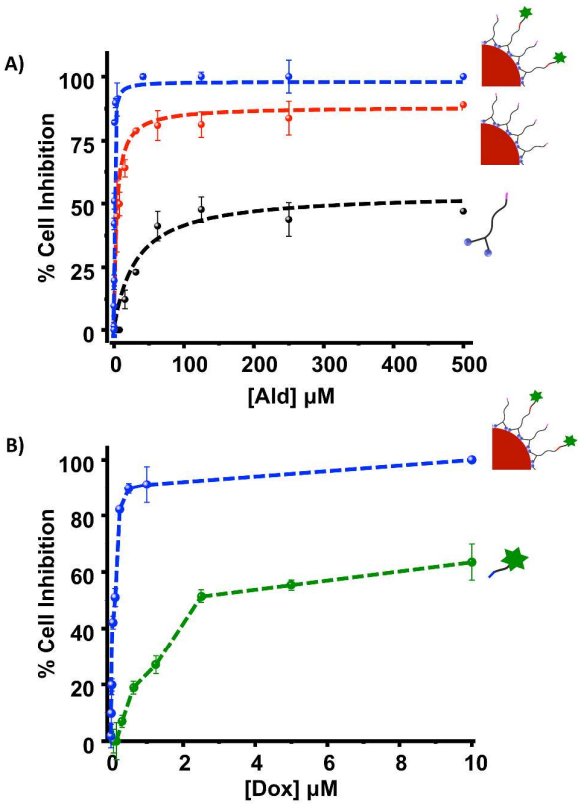

Fig. 8. (A) Inhibition of HeLa cell proliferation after 48 hours as a function of molar concentration of Ald, where Ald was added as free Ald (black curve), Ald@AgNPs (red curve), or Dox-Ald@AgNPs (blue curve). (B) Inhibition of HeLa cell proliferation after 48 h as a function of the molar concentration of Dox, where Dox was added as free Dox (green curve) or Dox-Ald@AgNPs (blue curve).

As expected, free Ald exhibited partial inhibition of cancer cell growth, with a maximum inhibition of 47% at 500 μM (Fig. 8A, black curve). With respect to the molar concentration of Ald, Ald@AgNPs (IC_{50} = 10.1 μM) were significantly more toxic (Fig. 8A, red curve). This increase might be due, in part, to the greater lipophilicity and consequent cellular uptake of Ald@AgNPs relative to free Ald. The greater toxicity of Ald@AgNPs is also consistent with previous results[43] that show that AgNPs have intrinsic anticancer properties and can induce apoptosis in HeLa cells. In our own experiments, we found that the IC_{50} of starch-coated AgNPs was 27 μM (Supporting Information).[42] With respect to the molar concentration of Ald, the anti-proliferative activity of Dox-Ald@AgNPs (Fig. 8A, blue curve) was 20 times greater (IC_{50} = 0.5 μM) than that of Ald@AgNPs (Fig. 8A, red curve). This enhancement can be attributed to the toxicity of Dox itself, which had an IC_{50} of 3 μM against HeLa cells (Figure 8B, green curve). With respect to the molar concentration of Dox, the anti-proliferative activity of Dox-Ald@AgNPs (Fig. 8B, blue curve) was 30 times greater (IC_{50} = 0.1 μM) than that of free Dox. Taken together, these results demonstrate the effectiveness of drug co-delivery, which in this case significantly increased the therapeutic indices of both Ald and Dox.

Two drugs are said to act synergistically when their combined effect is greater than the sum of the effects from each drug individually. Synergistic combinations allow for reduced drug dosing, minimized toxicity and fewer side effects. Chou and Talalay introduced[44] the concept of the combination index (CI) for evaluating the effectiveness of drug combinations. On this scale, CI > 1, CI = 1 and CI < 1 indicate antagonism, additive effects, and synergism, respectively. For the Dox-Ald@AgNP system, we calculated (see the Supporting Information for details) a CI value of 0.05, which reflects significant synergism.

Conclusions

We have developed a technically simple method for the synthesis of Ald@AgNPs that act as a pH-responsive dual drug-delivery system. The synthesis relies on water, activated by microwave radiation, as the sole reducing agent and avoids the use of cytotoxic or difficult-to-remove reagents. Ald@AgNPs were characterized by TGA; FTIR and UV-Vis absorption spectroscopies; fluorescence emission spectroscopy; and ζ-potential measurements; and in SEM, PXRD, and EDX experiments. The optimized synthetic method produces size-controlled Ald@NPs with enhanced colloidal stability. Ammonium groups decorate the surface of the Ald@AgNPs and allow for attachment of functional molecules such as dyes and drugs. Cell-permeability studies involving RhB@AgNPs showed that the main cellular uptake routes of the particles are macropinocytosis and clatharin-mediated endocytosis. We attached Dox to Ald@AgNPs and studied the drug's pH-triggered release in HeLa cells. Dox was released in late endosomes/lysosomes and became evenly distributed throughout the cytosol. AgNPs, Ald and Dox are, individually, antiproliferative. In the Ald@AgNP and Dox-Ald@AgNP systems, synergistic effects against HeLa cells were apparent. The therapeutic effect of Ald was enhanced by a factor of 50 by attachment to AgNPs, and that of Dox was enhanced by a factor of 30 when attached to Ald@AgNPs. Thus, the Dox-Ald@AgNP construct could avoid the problem of low therapeutic index, which hampers the use of many current cancer drugs. Furthermore, as a combination therapy, Dox-Ald@AgNP could potentially avoid, or at least delay, the onset of drug resistance. We are continuing to develop the Dox-Ald@AgNP system as a candidate anticancer therapeutic. We are also devising methods for attaching other drugs as well as cell-targeting agents to the Ald@AgNP delivery platform.

Acknowledgements

The research described here was sponsored by New York University Abu Dhabi (NYUAD), UAE. F.B., R.R., T.J., M.M., and A.T. thank NYUAD for their generous support for the research

program at NYUAD. This research was carried out by using the Core Technology Platform resources at NYUAD. The authors thank Dr Erwan Guenin for providing the diesterified Alendronate.

References

1 a) B. A. Teicher, E. A. Sotomayor and Z. D. Huang, *Cancer Res.*, 1992, **52**, 6702-6704; b) A. Yagoda and D. Petrylak, *Cancer*, 1993, **71**, 1098-1109; c) M. Pegram, S. Hsu, G. Lewis, R. Pietras, M. Beryt, M. Sliwkowski, D. Coombs, D. Baly, F. Kabbinavar and D. Slamon, *Oncogene*, 1999, **18**, 2241-2251; d) T. Browder, C. E. Butterfield, B. M. Kraling, B. Shi, B. Marshall, M. S. O'Reilly and J. Folkman, *Cancer Res.*, 2000, **60**, 1878-1886.
2 S. R. MacEwan, D. J. Callahan and A. Chilkoti, *Nanomedicine*, 2010, **5**, 793-806.
3 J. M. Owens, K. Fuller and T. J. Chambers, *J. Cell. Physiol*, 1997, **172**, 79-86.
4 M. Salerno, E. Cenni, C. Fotia, S. Avnet, D. Granchi, F. Castelli, D. Micieli, R. Pignatello, M. Capulli, N. Rucci, A. Angelucci, A. Del Fattore, A. Teti, N. Zini, A. Giunti and N. Baldini, *Curr. Cancer Drug Tar.*, 2010, **10**, 649-659.
5 a) L. S. Nair and C. T. Laurencin, *J. Biomei. Nanotechnol.*, 2007, **3**, 301-316; b) P. Jain, X. Huang, I. El-Sayed and M. El-Sayed, *Plasmonics*, 2007, **2**, 107-118.
6 P. Setua, A. Chakraborty, D. Seth, M. U. Bhatta, P. V. Satyam and N. Sarkar, *J. Phys. Chem. C*, 2007, **111**, 3901-3907.
7 Q. Yu, C. Liu, Z. Zhang and Y. Liu, *J. Phys.Chem. C*, 2008, **112**, 2266-2270.
8 A. Henglein and D. Meisel, *Langmuir*, 1998, **14**, 7392-7396.
9 H. Wang, X. Qiao, J. Chen and S. Ding, *Colloid Surface A*, 2005, **256**, 111-115.
10 A. Henglein and M. Giersig, *J. Phys. Chem. B*, 1999, **103**, 9533-9539.
11 D. L. Van Hyning and C. F. Zukoski, *Langmuir*, 1998, **14**, 7034-7046.
12 R. Hu, K. T. Yong, I. Roy, H. Ding, S. He and P. N. Prasad, *J. Phys. Chem. C, Nanomaterials and interfaces*, 2009, **113**, 2676-2684.
13 R. R. Arvizo, S. Bhattacharyya, R. A. Kudgus, K. Giri, R. Bhattacharya and P. Mukherjee, *Chem. Soc. Rev.*, 2012, **41**, 2943-2970.
14 A. Panacek, L. Kvitek, R. Prucek, M. Kolar, R. Vecerova, N. Pizurova, V. K. Sharma, T. Nevecna and R. Zboril, *J. Phys. Chem. B*, 2006, **110**, 16248-16253.
15 K. G. Stamplecoskie and J. C. Scaiano, *J. Am. Chem. Soc.*, 2010, **132**, 1825-1827.
16 A. E. Nel, L. Madler, D. Velegol, T. Xia, E. M. Hoek, P. Somasundaran, F. Klaessig, V. Castranova and M. Thompson, *Nat. Mater.*, 2009, **8**, 543-557.
17 A. Ediriwickrema and W. M. Saltzman, *ACS Biomaterials Science & Engineering*, 2015, **1**, 64-78.
18 P. Fiurasek and L. Reven, *Langmuir*, 2007, **23**, 2857-2866.
19 F. Benyettou, E. Guenin, Y. Lalatonne and L. Motte, *Nanotechnology*, 2011, **22**, 055102.
20 X. Liu, Y. Mou, S. Wu and H. C. Man, *Appl. Surf. Sci.*, 2013, **273**, 748-757.
21 a) J. Tao, J. P. Perdew, V. N. Staroverov and G. E. Scuseria, *Phys. Rev. Lett.*, 2003, **91**, 146401; b) Frisch, M. J.; Trucks, G. W.; Schlegel, H. B.; Scuseria, G. E.; Robb, M. A.; Cheeseman, J. R.; Scalmani, G.; Barone, V.; Mennucci, B.; Petersson, G. A. et al. Gaussian, Inc., Wallingford CT, **2009**.
22 D. Andrae, U. Häußermann, M. Dolg, H. Stoll and H. Preuß, *Theoret. Chim. Acta*, 1990, **77**, 123-141.
23 J. M. L. Martin and A. Sundermann, *J. Chem Phys.*, 2001, **114**, 3408-3420.
24 X. Lu and E. Masson, *Langmuir*, 2011, **27**, 3051-3058.
25 V. V. Srabionyan, A. L. Bugaev, V. V. Pryadchenko, A. V. Makhiboroda, E. B. Rusakova, L. A. Avakyan, R. Schneider, M. Dubiel and L. A. Bugaev, *J. Non-Cryst. Solids*, 2013, **382**, 24-31.
26 a) F. Benyettou, Y. Lalatonne, I. Chebbi, M. Di Benedetto, J. M. Serfaty, M. Lecouvey and L. Motte, *Phys. Chem. Chem. Phys.,*, 2011, **13**, 10020-10027 ; b) Y. Lalatonne, C. Paris, J. M. Serfaty, P. Weinmann, M. Lecouvey and L. Motte, *Chem. Commun*, 2008, 2553-2555; R. Aufaure, Y. Lalatonne, N. Lievre, O. Heintz, L. Motte and E. Guenin, *RSC Advances*, 2014, **4**, 59315-59322.
27 V. L. Vaks, G. A. Domrachev, Y. L. Rodygin, D. A. Selivanovskii and E. I. Spivak, *Radiophys Quantum El.*, 1994, **37**, 85-88.
28 T. Linnert, P. Mulvaney, A. Henglein and H. Weller, *J. Am. Chem. Soc.*, 1990, **112**, 4657-4664.
29 J. Jortner and R. M. Noyes, *J. Phys. Chem.*, 1966, **70**, 770-774.
30 B. G. Ershov and E. V. Abkhalimov, *Colloid J*, 2007, **69**, 579-584.
31 E. Guénin, M. Monteil, N. Bouchemal, T. Prangé and M. Lecouvey, *Eur. J. Org. Chem.*, 2007, **2007**, 3380-3391.
32 M. Meloun, Z. Ferenčíková, L. Netolická and T. Pekárek, *J. Chem. Eng. Data*, 2011, **56**, 3848-3854.
33 F. Benyettou, E. Guenin, Y. Lalatonne and L. Motte, *Nanotechnology*, 2011, **22**, 055102.
34 a) B. I. Ipe, K. G. Thomas, S. Barazzouk, S. Hotchandani and P. V. Kamat, *J. Phys. Chem. B*, 2002, **106**, 18-21; b) S. Ghosh, U. Anand and S. Mukherjee, *Analyst*, 2013, **138**, 4270-4274.
35 E. Dulkeith, A. C. Morteani, T. Niedereichholz, T. A. Klar, J. Feldmann, S. A. Levi, F. C. van Veggel, D. N. Reinhoudt, M. Moller and D. I. Gittins, *Phys. Rev. Lett.*, 2002, **89**, 203002.
36 .B. Kang, M. M. Afifi, L. A. Austin and M. A. El-Sayed, *ACS nano*, 2013, **7**, 7420-7427.
37 T. Sun, Y. S. Zhang, B. Pang, D. C. Hyun, M. Yang and Y. Xia, *Angew. Chem. Int. Ed.*, 2014, **53**, 12320-12364.
38 M. Rodrigues, B. G. de la Torre, D. Andreu and N. C. Santos, *Biochim Biophys Acta*, 2013, **1830**, 4554-4563.
39 R. D. Phair and T. Misteli, *Nature*, 2000, **404**, 604-609.
40 Y. Zhang, H. Peng, W. Huang, Y. Zhou and D. Yan, *J. Colloid. Interf. Sci.*, 2008, **325**, 371-376.
41 C. Greulich, J. Diendorf, T. Simon, G. Eggeler, M. Epple and M. Koller, *Acta Biomater.*, 2011, **7**, 347-354.
42 Silver nanoparticles coated with starch, which is non-toxic, were prepared as described in Kahrilas *et al. ACS Sustainable Chem. Eng.*, 2014, **2**, 590–598. The particles were added to HeLa cell culture, and after 48 hours of incubation, cell viability was considerably reduced. The IC_{50} of the particles was found to be 27 µM.
43 T. Kim and T. Hyeon, *Nanotechnology*, 2014, **25**, 012001.
44 a) T.-C. Chou, *Cancer Res.*, 2010, **70**, 440-446; b) T.-C. Chou and P. Talalay, *Adv. Enzyme Regul.*, 1984, **22**, 27-55.

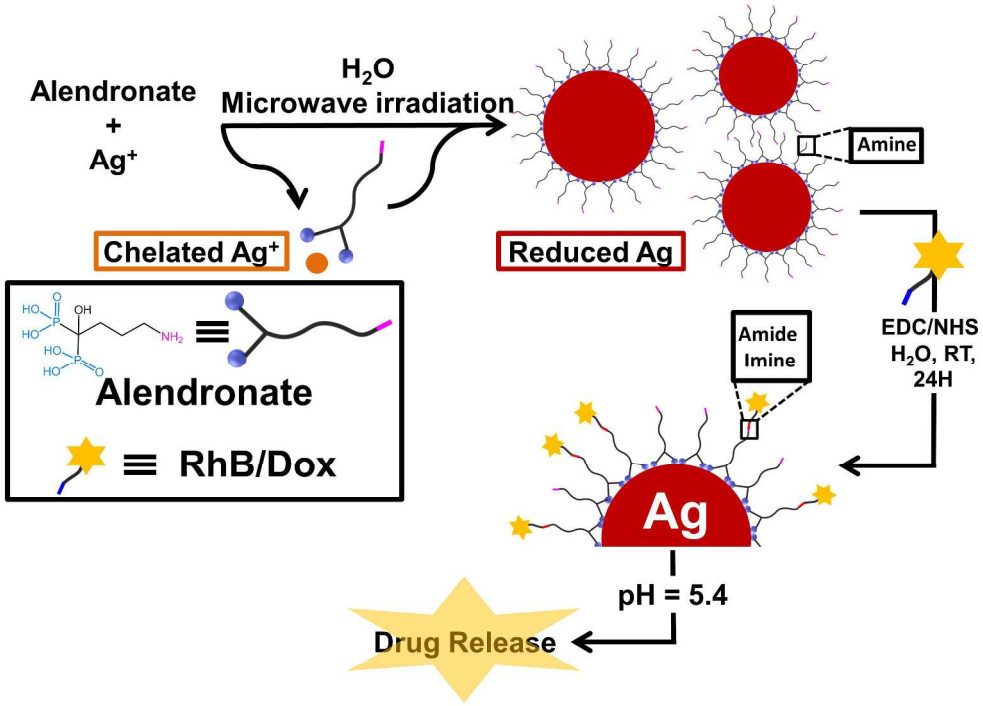

1418x1418mm (55 x 55 DPI)